



Delegation of Austria

XIII-2584-15

Effect of loading type on welded and HFMI-treated T-joints

M. Ottersböck¹, M. Leitner¹ and M. Stoschka¹

¹Montanuniversität Leoben, Department Product Engineering,
Chair of Mechanical Engineering, Austria

Abstract

Fatigue strength of welded components is generally susceptible to various load types, such as tension/compression, bending, or torsion loading during operation. In most cases, a combination of loading types is mainly considered using equivalent stresses, which is then compared to fatigue resistance values obtained by uniaxial specimen test results. To gain additional insight into this topic, this work deals with the effect of base plate bending versus tension loading on the fatigue strength of non-load carrying transversal joints.

Fatigue tests of T-joints in bending mode are carried out for two different steel grades, S355 and S690, exhibiting a common sheet thickness of 5 mm in the as-welded and the HFMI-treated condition. Compared to tension loading, the nominal stress fatigue test results show that bending loading leads to a significantly lower fatigue strength in case of as-welded condition. Both loading type dependent results are still above the IIW-recommended design S/N-curve, even if a benign thinness bonus factor is applied. On the other hand, the HFMI-treatment of the T-joints leads to a distinct improvement of the fatigue resistance under bending loading. This applies for both steel grades considered in the experimental investigations, although it is more pronounced in case of the common construction steel grade S355.

Numerical simulations are performed for bending and tension loading in order to calculate the stress concentration factor and local relative stress gradient at the weld toe for various weld toe radii ranging from 0.05 mm to 3 mm. The numerical investigations indicate a distinct influence of the loading type on the stress concentration factor. Furthermore, the weld toe radius has a significantly influence on both evaluated parameters. A lower radius leads to higher values of both local parameters, whereat the stress gradient illustrates an even sharper increase.

A fatigue assessment based on the critical distance, fictitious notch rounding, and local stress gradient approach is performed in order to clarify if these concepts are suitable for welded and HFMI-treated T-joints under tension and bending loading. Thereby, the obtained result for tension loading demonstrates a good accordance to the test results in the as-welded condition. However, for HFMI post-treated specimen a major deviation in fatigue strength is observed. Fatigue of bending loaded joints is not properly accessible by these methods. However, effective stress based design methods might be more suitable to cover the effect of loading on fatigue strength.

Keywords: Fatigue strength, Welded joints, High frequency mechanical impact (HFMI) treatment, Loading type, Microstructural support effect

1 Introduction

In the recommendation of the International Institute of Welding (IIW) [1], a combination of loading types is mainly considered on the basis of equivalent stresses. In most of the cases the calculated equivalent stress is then compared to fatigue resistance values obtained by cyclic tension tests. Various welded structures, for example cranes or railway vehicles are exposed to bending loading during their service life. Within these applications, lightweight design plays an important role to meet economic and legal targets. Therefore, a more precise knowledge of the bending fatigue behaviour of welded joints is of interest. For a more thorough view on this topic, this work deals with the effect of base plate bending loading on the fatigue strength of non-load carrying transversal T-joints. Experimental investigations are performed using a four-point bending device to gain the fatigue strength of as-welded as well as HFMI-treated T-joints. On the other hand, numerical simulations are carried out to identify the differences between tensile and bending loading based on linear elastic material behaviour.

As bending and tensile loading creates a normal stress state both loading types can be superposed. The main difference in the stress condition between tensile and bending can be found in the through-sheet stress distribution. For unnotched components, tensile loads imply a constant stress course, whereas bending leads to a linear distribution with a neutral axis in the centre. According to [1], the stress distribution in welded joints can be separated to a membrane stress σ_m , a shell bending stress σ_b and a non-linear stress peak σ_{nl} (Equations 1-3).

$$\sigma_m = \frac{1}{t} \int_{x=0}^{x=t} \sigma(x) dx \quad \text{Equ. 1}$$

$$\sigma_b = \frac{6}{t^2} \int_{x=0}^{x=t} [\sigma(x) - \sigma_m] \left(\frac{t}{2} - x \right) dx \quad \text{Equ. 2}$$

$$\sigma_{nl} = \sigma(x) - \sigma_m - \left(1 - \frac{2x}{t} \right) \sigma_b \quad \text{Equ. 3}$$

For non-welded components numerous publications show a significant influence of the loading type on the fatigue strength of the material [2, 3]. There are various concepts to take this “support effect” into account. In [4], among others four different concepts are discussed:

- Critical distance approach by Peterson [5]
- Stress averaging approach originally by Neuber [6, 7]
- Stress gradient approach by Siebel and Stieler [8]
- Highly stressed volume approach originally by Kuguel [9]

In this work, the applicability of these concepts for welded and HFMI-treated T-joints under tension and bending loading based on fatigue test results is investigated.

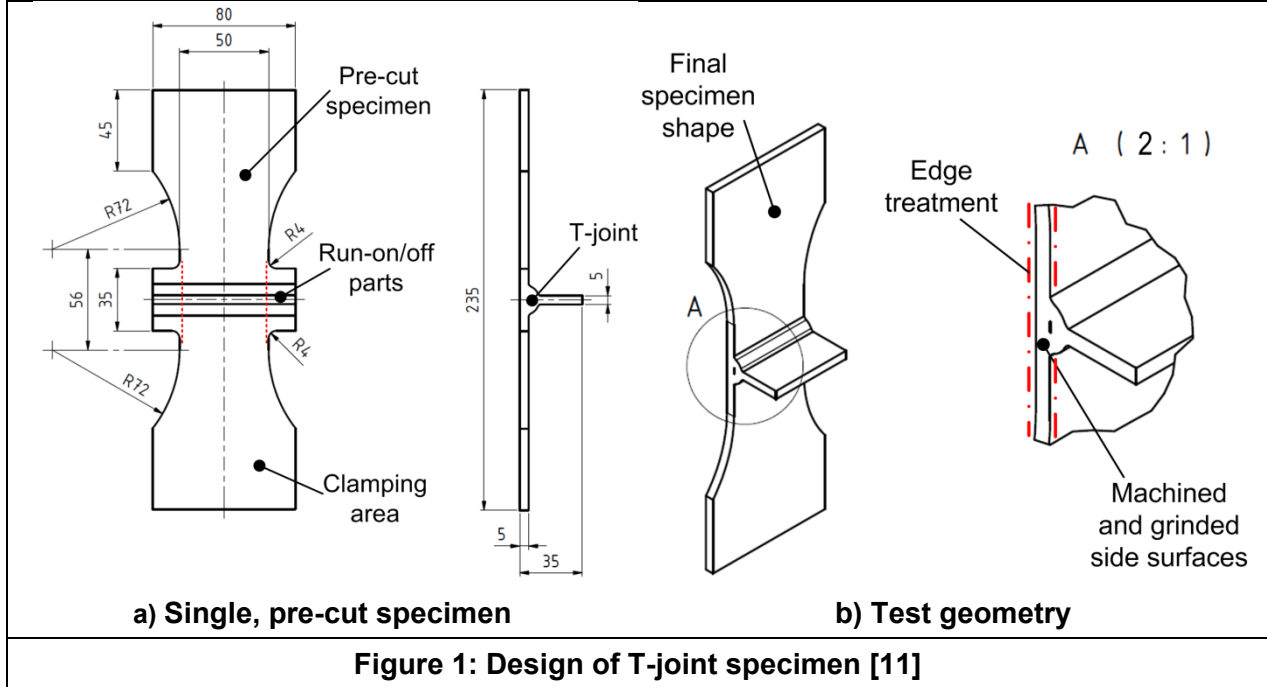
2 Fatigue tests

The experimental investigations cover fatigue testing of welded and HFMI-treated T-joints under bending load. Subsequently, the obtained test results are compared to results under tension load [10]. In this work, specimen with 5 mm sheet thickness with steel grades of mild steel S355 and high-strength steel S690 in as-welded and HFMI-treated condition are tested. The fatigue tests are performed using a bending device installed on a high frequency resonator at a nominal stress ratio of $R=0.1$.

2.1 Specimen manufacturing

The specimen manufacturing is conducted according to [11] in order to ensure comparability of the fatigue test results. This means the steel sheets are sliced to specimen arrays of eight single specimens using water-jet cutting before welding. An illustration of the specimen design is shown in Figure 1. Each array is welded continuously to ensure a constant welding process over every specimen. Although fatigue testing in

bending mode is not very sensitive to longitudinal welding distortion, a filler wire is placed beneath the array before final clamping to counteract a too high angular weld distortion. In [11] and [12] distortion measurements verified, that this procedure leads to specimen with quite low distortion values. The HFMI post-treatment is done using the PIT-device [13] with process parameters given in [14]. After truncating of the arrays into single specimens, the side surfaces are machined and ground flush to obtain the final specimen shape. For the prevention of unfavourable crack initiation from sheet edges, slight compressive residual stresses are induced by mechanical treatment.



2.2 Bending device

For the conversion of the linear resonance pulsator force to a bending load an elaborated bending device is used, see Figure 2. Thereby, the 4-point-bending principle ensures a constant bending moment over the structural weld detail. The specimen is loaded via four pivoted rolls, whereby the contact areas are lubricated for minimisation of friction. Additionally, the lower portion of the device is additionally pivoted to assure symmetric contact condition in case of longitudinally distorted specimen.

The dimensions a and c of the device are selected based on preceding numerical simulations to guarantee the operability operation on the chosen resonance pulsator. Therefore, the main focus within these preliminary analyses was to assess the required force to reach a certain maximum stress range in dependence of the resulting maximum displacement during testing. As thin-walled specimens are comparable flexible and the minimum force amplitude of the pulsator is limited, the resulting device measures with values of $a=140\text{ mm}$ and $c=60\text{ mm}$ are obtained by several iterations. The bending device operates on an unbalanced-mass-driven resonant test rig which supports a displacement amplitude up to one millimetre. This makes the bending device suitable for steel sheet thicknesses from five to fifteen millimetres.

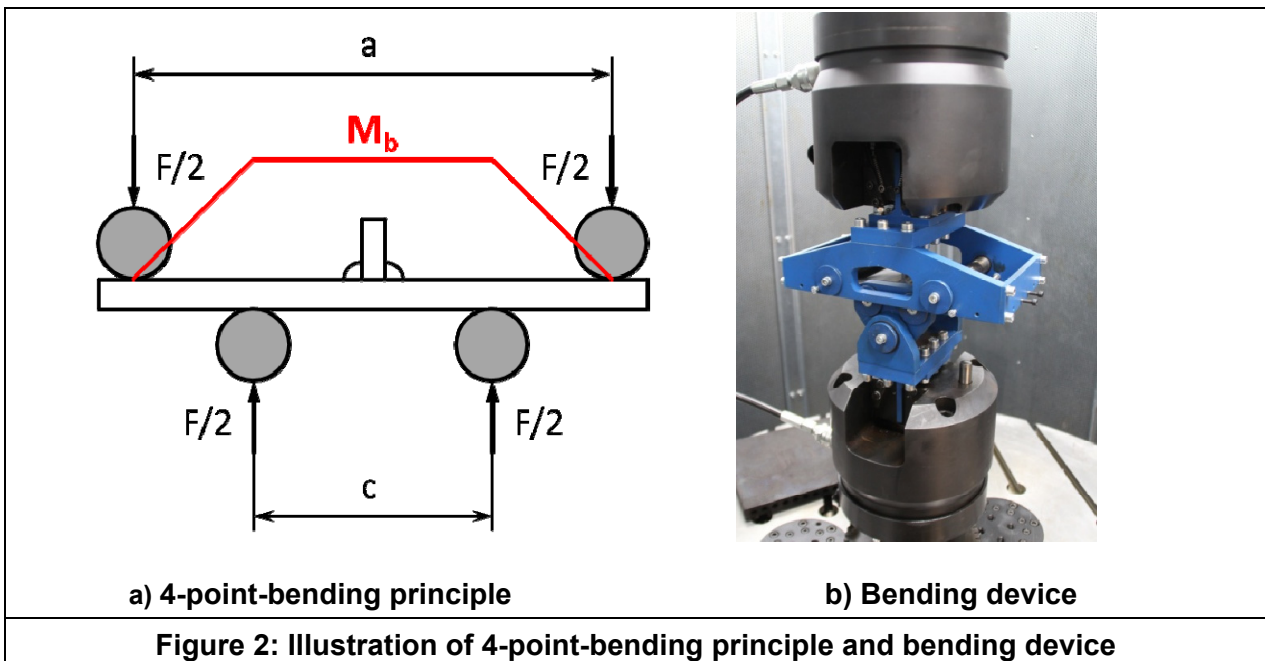


Figure 2: Illustration of 4-point-bending principle and bending device

2.3 Fatigue test results

Overall 125 specimens are tested to examine the effect of bending load on the fatigue strength of welded and HFMI-treated joints. The evaluation of the fatigue test data in the finite life region is done according to ASTM E739 [15]. For bending tests the run-out level is set to $2 \cdot 10^7$ load cycles, the tension test results from [10] are tested up to a run-out level of $5 \cdot 10^7$ load cycles. The statistical analysis of the run-out level is performed using the arcsin \sqrt{P} -transformation [16]. The evaluation of the finite life domain is performed based on a variable slope. In contrary, at the high-cycle fatigue region a constant decay of 10% per decade corresponding to a inverse slope value of $k=22$ is assumed as recommended in [1].

Figure 3 shows the fatigue test results for mild construction steel S355 in terms of nominal stresses. For the as-welded specimen bending loads exhibits a significantly loss on fatigue strength. This can be reasoned due to a steeper slope k indicating a sharper notch factor as well as on an increase of the transition knee point N_k . Furthermore, the run-out level is essentially lower for bending than for tension load. In contrast, in the low-cycle fatigue region below $5 \cdot 10^4$ load cycles, specimens subjected to bending loading manifest a slightly higher fatigue strength. Fatigue test results in tension show that the HFMI treatment does not have a significant influence on the fatigue behaviour, especially in case of the investigated mild steel S355. On the other hand, the post-treated specimens under bending load show a major increase in fatigue strength, far higher compared to tension. Considering the run-out level at $2 \cdot 10^7$ load-cycles, the raise in fatigue strength equals about 115% compared to as-welded bending specimen and 34% compared to HFMI-treated tension specimen.

In Figure 4 the fatigue test results for the high-strength steel S690 joint in terms of nominal stresses are depicted. The as-welded bending specimen exhibit similar to the results of S355 the lowest fatigue strength. However, the difference to tension loading is less pronounced. In the finite life domain the deviations are negligible, whereas a difference of about 10% can be obtained at run-out level. The HFMI treatment shows the same effect as for the mild steel S355. The HFMI-treated bending specimens show the highest fatigue strength. In particular, at the run-out load-level an increase of about 60% in comparison to as-welded bending and about 12% to HFMI-treated tension specimen is observed.

Summing up, the results of the experimental investigations show a decrease in fatigue strength of as-welded joints under bending based on nominal stress assessment. On the other hand, HFMI treatment of the weld toe leads to a complete reversal of this situation. It is interesting to note, that the common construction steel joint shows a major increase in fatigue strength for HFMI-treated bending specimen, but almost no improvement in case of tension.

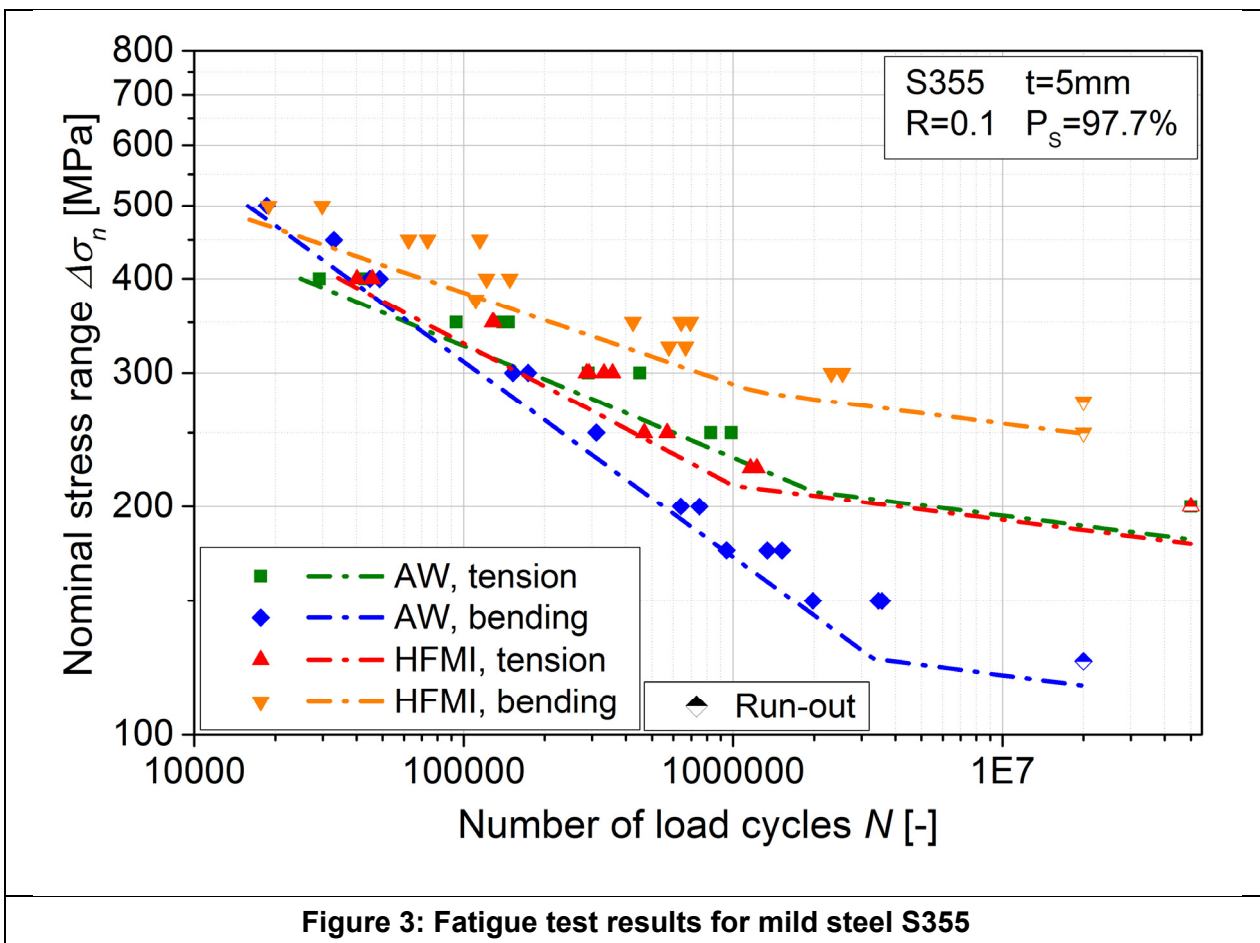


Figure 3: Fatigue test results for mild steel S355

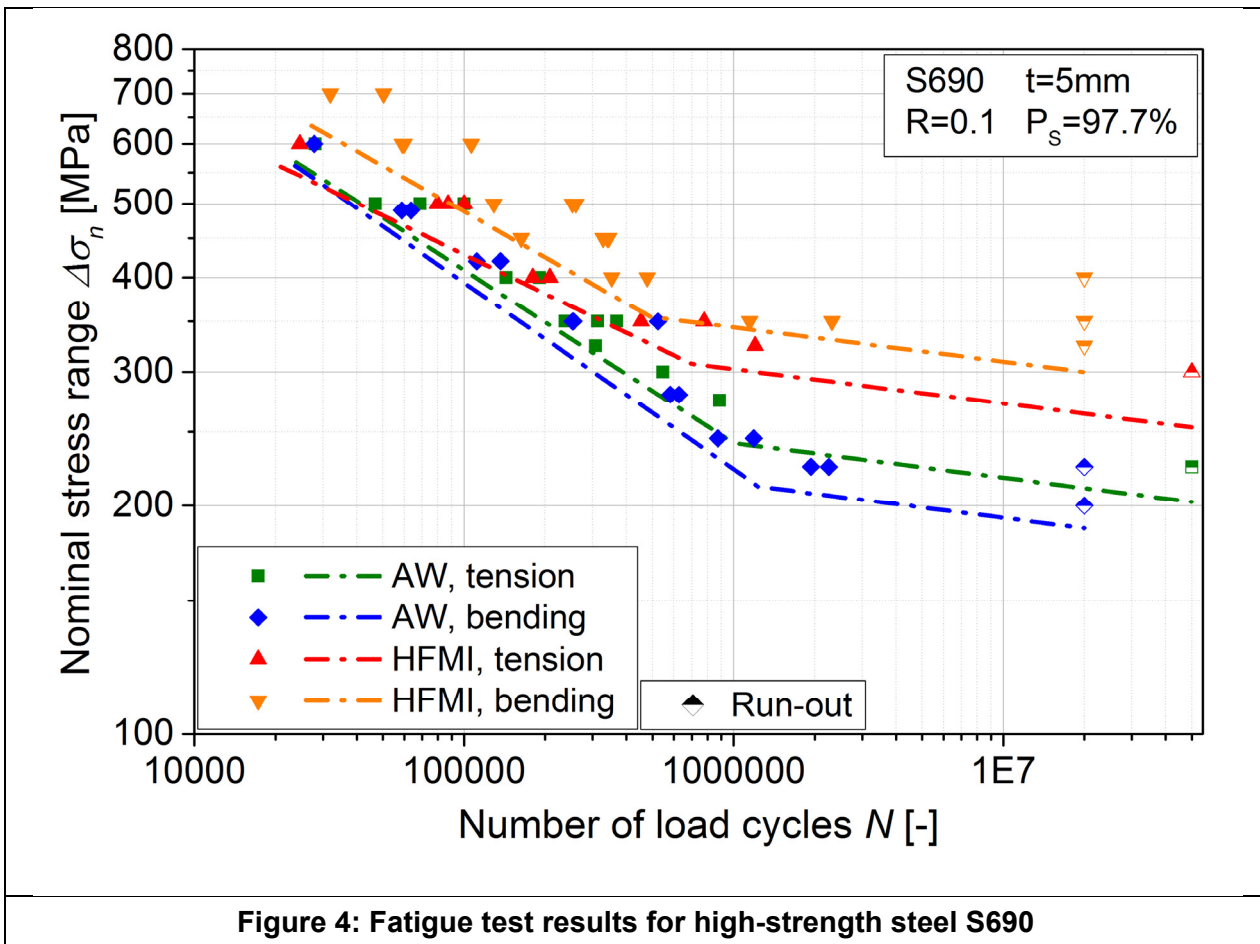


Figure 4: Fatigue test results for high-strength steel S690

Table 1 summarizes the parameters of the statistically evaluated S/N-curves for the investigated S355 and S690 T-joint specimens.

Table 1: Summary of fatigue test results

Steel grade	Loading type	Condition	Slope k	Scatter range $1:T_\sigma$	Transition knee point N_k	$\Delta\sigma_n$		
						$N=2 \cdot 10^6$		$N=2 \cdot 10^7$
						[MPa]	[MPa]	[%]
S355	Tension	Base material	7.6	1.07	$1.5 \cdot 10^6$	250	250	-
		As-welded	6.8	1.11	$2 \cdot 10^6$	210	188	100
		HFMI-treated	5.3	1.12	$1 \cdot 10^6$	187	186	99
	Bending	As-welded	3.9	1.09	$3.3 \cdot 10^6$	144	116	62
		HFMI-treated	8.2	1.14	$1.2 \cdot 10^6$	266	249	132
S690	Tension	Base material	3.9	1.13	$0.8 \cdot 10^6$	280	280	
		As-welded	4.4	1.11	$1 \cdot 10^6$	206	210	100
		HFMI-treated	5.9	1.13	$0.7 \cdot 10^6$	257	264	126
	Bending	As-welded	4.1	1.15	$1.2 \cdot 10^6$	188	187	89
		HFMI-treated	5.0	1.21	$0.5 \cdot 10^6$	268	300	143

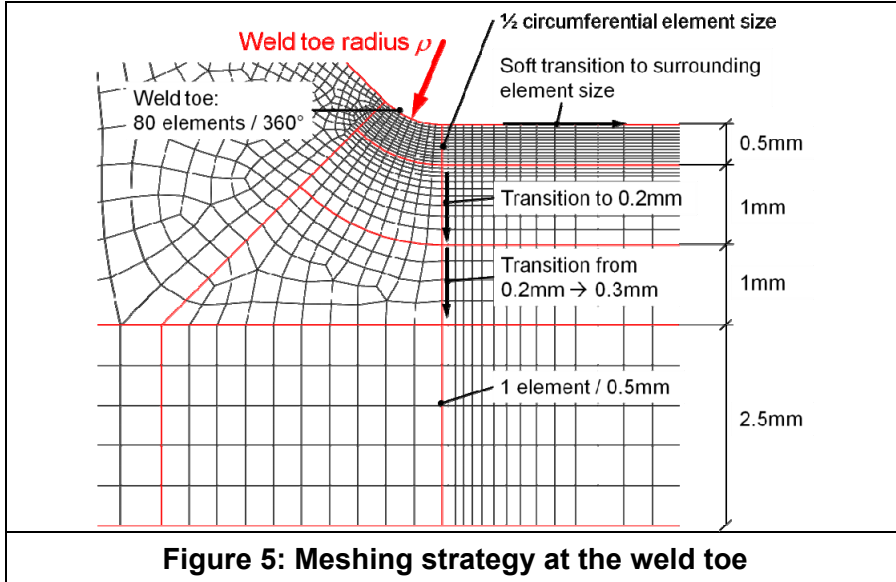
3 Numerical analysis

For the determination of the stress concentration factor K_t and the local relative stress gradient χ^* , linear elastic finite element analysis are carried out for tension and bending load. Main focus of the numerical work is laid on the influence of the weld toe radius on the calculated local fatigue strength assessment parameters. Thereby, the element size possesses a significant influence on the results of the numerical analyses; especially the relative stress gradient shows a high sensitivity to the mesh seed. Hence, an adequate meshing strategy at the notch region is worked out, whereby the element size at the notch remains constant relative to the notch radius. A three-dimensional, quarter-symmetric model of the T-joint is used for all investigations. The element type is a 20-node hexaeder with quadratic shape function and reduced integration scheme. All models are stressed with a uniform load resulting in a nominal stress of 1 MPa.

3.1 Meshing strategy

As stated, the element size exhibits a significant influence on the result of numerical simulations, see [17]. In particular the local relative stress gradient shows sensitivity to the absolute size of the elements. Naturally, smaller elements lead to a higher gradient. Thus, the calculations are more precise the larger the weld toe radius ρ is modelled, if the absolute element size remains constant. Therefore, a meshing strategy is set up to ensure a constant quality of the mesh for all models.

Figure 5 shows the meshing strategy for the analysis. At the weld toe 80 elements per 360° are selected while in depth, the element size is defined half of the element length in circumferential direction. This leads to an improved approximation of the stress gradient without a disproportionate increase of number of elements.

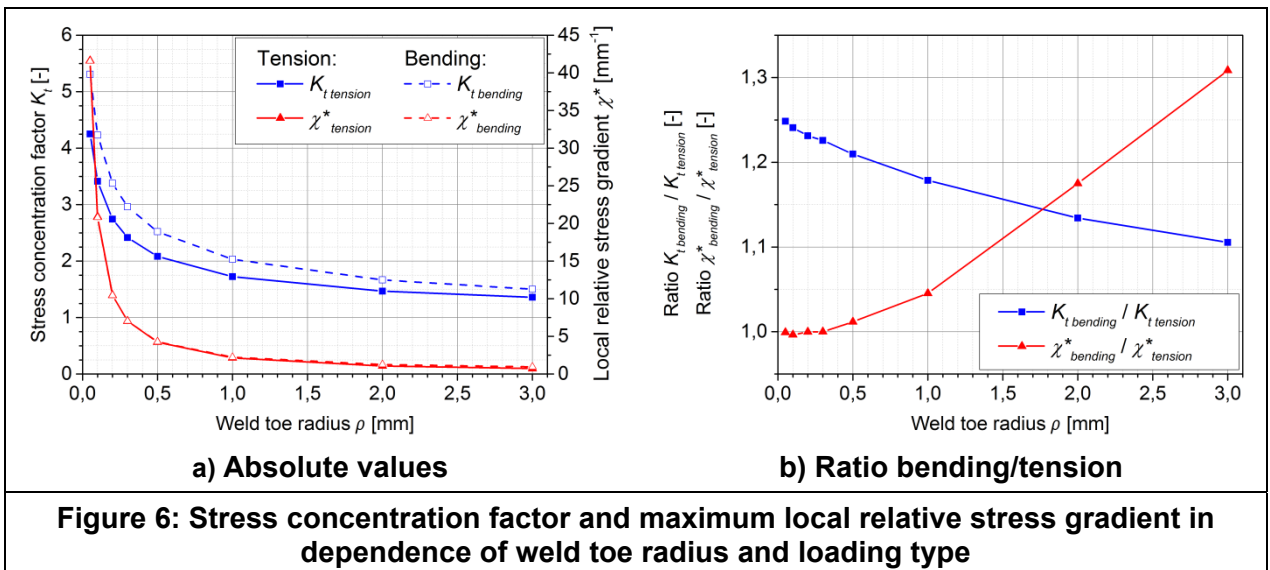


3.2 Influence of the weld toe radius

The given meshing strategy is used to set up eight models with different weld toe radii and a sheet thickness of $t=5\text{ mm}$ for bending and tensile load. A variation of the weld toe radius ρ provides an overview of its effect on the evaluated parameters. The specific values are selected from a crack-like notch with $\rho=0.05\text{ mm}$, as recommended for thin metal sheets [18], up to $\rho=2\text{ to }3\text{ mm}$ representing the geometry of post-treated weld toes. The evaluated values, stress concentration factor K_t and the maximum local relative stress gradient χ^* , are performed using equations 4 and 5 in section 4. Figure 6 shows the development of the calculated parameters in absolute and relative values; Table 2 lists the related numbers.

The stress concentration factor shows in general higher values for bending compared to tension loading. Thereby, the ratio $K_{t\text{ bending}} / K_{t\text{ tension}}$ shows indirect proportional behaviour to the weld toe radius, but even for the smallest analysed radii of $\rho=0.05\text{ mm}$ a ratio of 1.25 is not exceeded.

The absolute values of the maximum local relative stress gradient show a significantly stronger dependence on the toe radius. Especially at comparable low toe radii a strong increase is observed. The local relative stress gradient depends on the global stress gradient and the stress gradient resulting from the local notch geometry. At small weld toe radii, the ratio $\chi^*_{\text{bending}} / \chi^*_{\text{tension}}$ equals about one. This effect can be traced back to the large influence of the local notch geometry on the local stress gradient in comparison to the global stress gradient. Hence, the local relative stress gradient is not applicable for sharp notches. With increasing weld toe radius the ratio $\chi^*_{\text{bending}} / \chi^*_{\text{tension}}$ increases to values of about 1.3 for a weld toe radius of 3 mm.



In Table 2 the results of the numerical investigations are summarised.

Table 2: Summary of numerical results

Weld toe radius [mm]	Stress concentration factor $K_t [-]$			Maximum local relative stress gradient $\chi^* [\text{mm}^{-1}]$		
	Tension	Bending	Bending / tension	Tension	Bending	Bending / tension
0.05	4.252	5.308	1.248	41.622	41.586	0.999
0.1	3.412	4.234	1.241	20.876	20.801	0.996
0.2	2.743	3.378	1.231	10.455	10.452	1.000
0.3	2.417	2.963	1.226	7.031	7.031	1.000
0.5	2.084	2.521	1.210	4.236	4.285	1.012
1.0	1.724	2.032	1.179	2.140	2.241	1.045
2.0	1.469	1.666	1.134	1.070	1.257	1.175
3.0	1.358	1.501	1.105	0.726	0.949	1.308

4 Fatigue assessment

Notches, such as holes, grooves or even mechanical joints lead to an increase of the local stress condition. This circumstance can be described by the stress concentration factor K_t . is defined as the ratio of the maximum notch to the nominal stress, see equation 4. The reduction of the fatigue strength along with a notch is naturally determined experimentally. It can be expressed by the fatigue notch factor K_f , see equation 5. Generally, for technical materials, K_f is smaller than K_t meaning that the maximum notch stress σ_{max} does not have a full effect in terms of fatigue. This effect is called microstructural support effect and is defined by the local notch support factor n_σ according to equation 6.

$$K_t = \frac{\sigma_{max}}{\sigma_n} \quad \text{Equ. 4}$$

$$K_f = \frac{\sigma_{n-unnotched}}{\sigma_{n-notched}} \quad \text{Equ. 5}$$

$$n_\sigma = \frac{K_t}{K_f} \quad \text{Equ. 6}$$

4.1 Overview on microstructural notch support hypotheses

In [4] the four mainly applied microstructural support hypotheses are described in detail as listed in section 1. With exception of the highly stressed volume approach, the hypotheses require only the stress concentration factor and/or the local relative stress gradient in combination with material parameters. The following subsections give a short overview on the approaches used in this work. The basic principle of all this concepts is the calculation of the fatigue notch factor K_f based on material and local loading parameters defining the local stress state.

4.1.1 Critical distance approach

This concept proposed by Peterson [5] introduces a material dependent critical distance a^* . The fatigue effective notch stress should be evaluated at this depth below the notch surface deriving the following equation with ρ as notch radius:

$$K_f = 1 + \frac{K_t - 1}{1 + a^*/\rho} \quad \text{Equ. 7}$$

The critical distance a^* is a material constant depending on the ultimate tensile strength σ_u of the material. In [19] Peterson provides values for a^* of steels with different ultimate tensile strength and Lawrence proposes an approximation for steels in [20]:

$$a^* = 0.025 \left(\frac{2068}{\sigma_u} \right)^{1.8} \quad \text{Equ. 8}$$

4.1.2 Fictitious notch rounding concept

This approach is derived by Radaj [21] based on Neuber's investigations in [7]. It is stated that instead the stress at notch root the averaged notch stress in a small material volume at the point of maximum stress controls the crack initiation. This material volume is described with a material constant named substitute microstructural support length ρ^* over which the stresses are averaged. The fatigue notch factor K_f is then derived with multiaxiality factor s and notch radius ρ as follows [22]:

$$K_f = 1 + \frac{K_t - 1}{\sqrt{1 + s\rho^*/\rho}} \quad \text{Equ. 9}$$

$$\rho_f = \rho + s\rho^* \quad \text{Equ. 10}$$

The substitute microstructural length ρ^* is considered to be dependent on the yield limit, whereat values are given in [7]. The factor s depends on the multiaxiality of the notch stress and the multiaxial strength criterion applied. If the determination of the stress concentration factor K_t is performed with a fictitious notch radius ρ_f resulting from the actual notch radius, s and ρ^* , the stress concentration factor represents directly the fatigue notch factor, thus avoiding the averaging process.

4.1.3 Local stress gradient approach

The microstructural support hypothesis based on a local stress gradient χ^* is originally proposed by Siebel and Stieler in [8], whereby χ^* is defined as following:

$$\chi^* = \frac{1}{\sigma_{max}} \frac{d\sigma}{dx} \quad \text{Equ. 11}$$

The main assumption of this concept applied in the FKM-guideline [23] is the dependence of the notch support factor n_σ , the ratio between K_f and K_t , on the local relative stress gradient. With ultimate tensile strength σ_u and two material parameters a_G and b_G it is defined as follows, whereby parameters for steel are $a_G=0.5$ and $b_G=2700$.

For $\chi^* \leq 0.1 \text{ mm}^{-1}$

$$n_\sigma = 1 + \chi^* \cdot \text{mm} \cdot 10^{-(a_G - 0.5 + \frac{\sigma_u}{b_G \cdot \text{MPa}})} \quad \text{Equ. 12}$$

For $0.1 \text{ mm}^{-1} \leq \chi^* \leq 1 \text{ mm}^{-1}$

$$n_\sigma = 1 + \sqrt{\chi^* \cdot \text{mm}} \cdot 10^{-(a_G + \frac{\sigma_u}{b_G \cdot \text{MPa}})} \quad \text{Equ. 13}$$

For $1 \text{ mm}^{-1} \leq \chi^* \leq 100 \text{ mm}^{-1}$

$$n_\sigma = 1 + \sqrt[4]{\chi^* \cdot \text{mm}} \cdot 10^{-(a_G + \frac{\sigma_u}{b_G \cdot \text{MPa}})} \quad \text{Equ. 14}$$

4.2 Microstructural support for tension loading

The microstructural support hypotheses listed in section 4.1 are basically valid for non-welded components. Thus, as a verification, a comparison to the tension fatigue test results from [10] is performed as there are also test results for base material available. Taking the stress concentration factors and relative gradients obtained in section 3.2, the particular fatigue notch factors for each concept are calculated. Subsequently, the nominal endurable fatigue stress range is calculated using equation 16 on the basis of the base material

endurance limit. The result is shown in Figure 7 depending on the weld toe radius for both investigated steel grades. It is clearly evident, that this simplified assessment of the fatigue strength of welded and HFMI-treated specimen based solely on test results of base material shows good agreement with the test results for the as-welded condition, whereat the recommended weld toe radius of $\rho=1 \text{ mm}$ produces conservative, but suitable fatigue strength values.

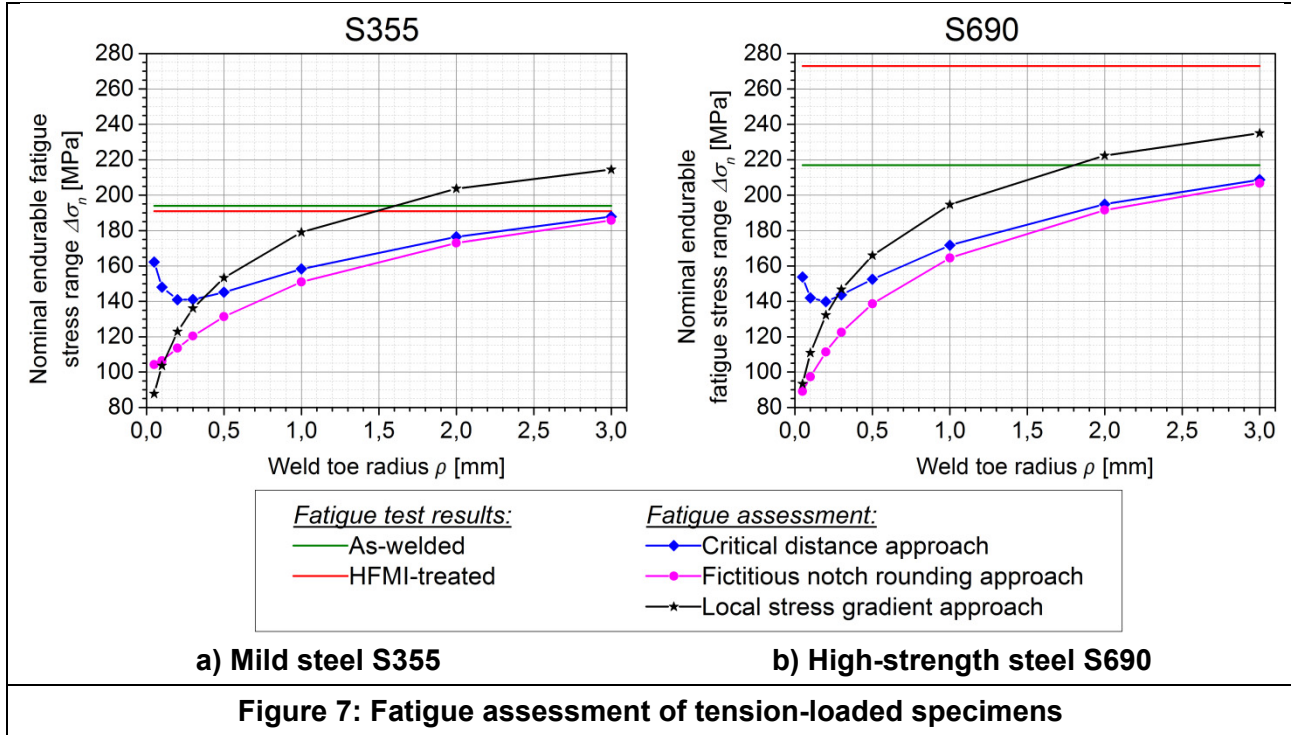


Figure 7: Fatigue assessment of tension-loaded specimens

4.3 Bending/Tension

The aim of the fatigue assessment in this work is a verification of the applicability of the approaches in section 4.1 for welded and HFMI-treated specimens in tension and bending load at the run-out load-level. It is questioned, if the results obtained for bending load can be estimated with one of these hypotheses based on the fatigue data from tension loading. Therefore, the ratio q of bending and tension fatigue strength $\Delta\sigma_{n \text{ weld bending}}$ and $\Delta\sigma_{n \text{ weld tension}}$ at run-out load-level is introduced.

$$q = \frac{\Delta\sigma_{n \text{ weld bending}}}{\Delta\sigma_{n \text{ weld tension}}} \quad \text{Equ. 15}$$

4.3.1 Fatigue strength ratio q for experiments

The fatigue notch factors K_f of the welded specimens are defined in equations 16 and 17 for tension and bending load.

$$K_{ftension} = \frac{\Delta\sigma_{n \text{ base tension}}}{\Delta\sigma_{n \text{ weld tension}}} \quad \text{Equ. 16}$$

$$K_{fbending} = \frac{\Delta\sigma_{n \text{ base bending}}}{\Delta\sigma_{n \text{ weld bending}}} \quad \text{Equ. 17}$$

The ratio q of bending and tension fatigue strength is derived by entering equations 16 and 17 in equation 15 thus eliminating the fatigue strength of the base material. Thereby, the local notch support factor $n_{\sigma \text{ base bending}}$ enables the conversion for base material from tension to bending. It is calculated with the stress gradient approach from the FKM-guideline [23].

$$q = \frac{K_{ftension}}{K_{fbending}} \cdot n_{\sigma \text{ base bending}}$$
Equ. 18

The values for q are listed in Table 3.

Table 3: Fatigue strength ratio q for experiments

S355		S690	
As-welded	HFMI-treated	As-welded	HFMI-treated
0.62	1.35	0.86	1.13

4.3.2 Calculation of fatigue strength ratio q

The values of q for the microstructural notch support approaches introduced in section 4.1 are listed in Table 4. Thereby, the calculation applies to the data obtained from numerical simulation listed in Table 2. The respective material parameters for each approach are determined considering an ultimate tensile strength $\sigma_u=575 \text{ MPa}$ for mild steel S355 and $\sigma_u=770 \text{ MPa}$ for high-strength steel S690 taken from [24].

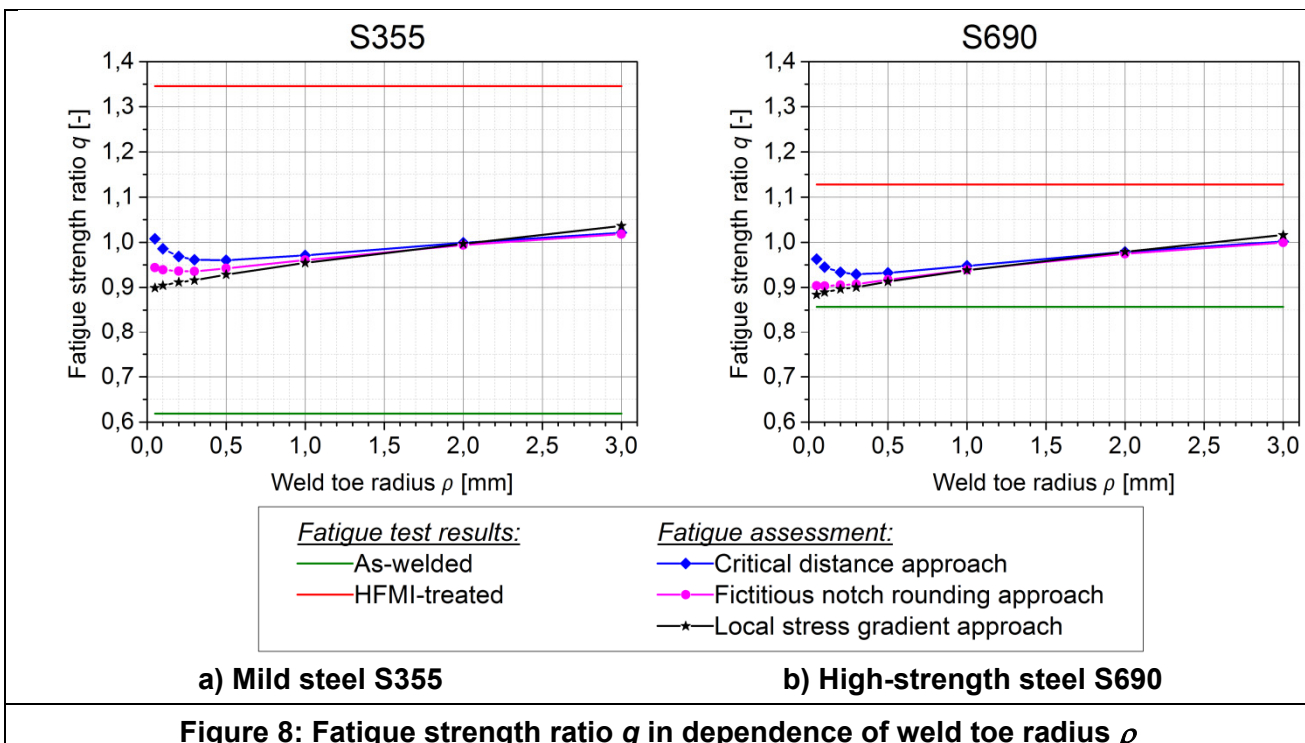
Table 4: Fatigue strength ratio q for local approaches

Weld toe radius [mm]	S355			S690		
	Critical distance approach	Fictitious notch rounding approach	Stress gradient approach	Critical distance approach	Fictitious notch rounding approach	Stress gradient approach
0.05	1.01	0.94	0.90	0.96	0.90	0.90
0.1	0.99	0.94	0.90	0.95	0.90	0.90
0.2	0.97	0.94	0.91	0.93	0.91	0.91
0.3	0.96	0.94	0.92	0.93	0.91	0.91
0.5	0.96	0.94	0.93	0.93	0.92	0.92
1.0	0.97	0.96	0.95	0.95	0.94	0.94
2.0	1.00	0.99	1.00	0.98	0.97	0.97
3.0	1.02	1.02	1.04	1.00	1.00	1.00

4.4 Comparison of experiments with local approaches

In Figure 8 the resulting values for the fatigue strength ratio q are plotted depending on the weld toe radius for both investigated materials. Thereby, in opposite to the fatigue strength results for tension load the calculated values do not agree with the experimental results. All hypotheses considered in the assessment lead to marginally lower nominal fatigue strength under bending. In contrast, the experiments show a significantly lower ratio q for as-welded condition and a significantly higher for the HFMI-treated state. This behaviour is far more pronounced among mild steel S355. The deviation of the average assessed fatigue strength for $\rho=1 \text{ mm}$ ($q=0.96$) from the as-welded fatigue strength is about 35%, from the HFMI-treated result approximately 41%. Evaluating high-strength steel S690, the difference is substantially lower by only 9% for the as-welded and 20% for the HFMI-treated state.

In general, the results of all evaluated approaches do not show a noticeable dependence on the weld toe radius. Fatigue strength under bending is not properly assessed by these approaches. As HFMI-treatment leads, upon other effects, to a substantial change of this radius, these concepts are not applicable for bending loaded HFMI-treated T-joints.



5 Summary and outlook

Fatigue tests of T-joints in bending mode are carried out for two different steel grades, S355 and S690, for a sheet thickness of 5 mm in as-welded and HFMI-treated condition. Therefore, a bending device is designed capable of testing the specimen on a resonance pulsator. The results are compared to fatigue test results obtained in tension loading to work out the influence of bending loading on the fatigue strength. Furthermore, numerical simulations are executed for bending and tension loading to calculate the stress concentration factor and local relative stress gradient at the weld toe. To figure out the influence of the weld toe radius on these parameters, various weld toe radii from 0.05 mm to 3 mm are investigated in numerical simulations. Finally, a fatigue assessment based on microstructural support hypotheses is performed to judge if the investigated approaches are suitable for welded T-joints in tension and bending loading.

The results of the fatigue tests show that bending loading leads to significantly lower fatigue strength within the whole S/N-curve in case of the as-welded condition. On the other hand, the HFMI-treatment of the specimen leads to a distinct improvement of the fatigue strength under bending compared to tension loading. These findings are valid for both steel grades considered in the experimental investigations, but however, mild steel S355 exhibits a more pronounced behaviour.

The numerical investigations show a distinct influence of the loading type on the stress concentration factor. Due to the higher section modulus at the transversal stiffener under bending, the fillet weld is more load-carrying compared to tension loading. Therefore, the bending loaded specimens exhibit an increase of about 10 to 20% in stress concentration. Basically, the weld toe radius has a significant influence on the stress concentration factor and the relative stress gradient.

Different microstructural support hypotheses are considered for the fatigue assessment, incorporating the critical distance, fictitious notch rounding, and local stress gradient method. At first, those approaches are used to assess the fatigue strength of tension loaded specimen based on the base material fatigue strength. The obtained results show a good accordance with the test results in as-welded condition. However, for HFMI-treated specimens a major deviation is observed. Subsequently, the ratio between evaluated fatigue strength for bending and tension loading is calculated based on the microstructural support hypotheses. Thus, by the aid of the investigated approaches, a consideration of bending loading leads to improper fatigue strength results for both, as-welded and HFMI-treated condition.

Future work deals with the application of more advanced approaches for the investigation of the effect on bending loading on the fatigue strength of welded and HFMI-treated joints such as the highly stressed volume concept or fracture mechanical based methods. In addition, the effective stress method offers an

interesting tool to assess the fatigue strength of welded joints with varying notch angles and notch radii. It will be studied if the concept in [25] is applicable for varying loading types as well. Furthermore, additional fatigue tests involving supplementary high-strength steel joints with different sheet thicknesses are scheduled, to investigate the influence of bending more in detail.

6 References

- [1] Hobbacher, A.: IIW Recommendations for Fatigue Design of Welded Joints and Components; *Welding Record Bulletin* 520 (2009).
- [2] Eichlseder, W.: Fatigue analysis by local stress concept based on finite element results; *Computers & Structures* 80 (2002)27-30, pp. 2109–2113.
- [3] Kloos, K. H.; Buch, A.; Zankov, D.: Pure Geometrical Size Effect in fatigue tests with constant stress amplitude and in programme tests; *Materialwissenschaft und Werkstofftechnik* 12 (1981)2, pp. 40–50.
- [4] Radaj, D.; Sonsino, C. M.; Fricke, W.: Fatigue assessment of welded joints by local approaches, Woodhead Publishing Ltd, 2006.
- [5] Peterson, R. E.: Relation between stress analysis and fatigue of metals; in *Proceedings of the Society of Experimental Stress Analysis* (Society for Experimental Stress Analysis Ed.), 1950, pp. 199–206.
- [6] Neuber, H.: Theory of Stress Concentration for Shear-Strained Prismatical Bodies With Arbitrary Nonlinear Stress-Strain Law; *Journal of Applied Mechanics* 28 (1961)4, pp. 544–550.
- [7] Neuber, H.: Über die Berücksichtigung der Spannungskonzentration bei Festigkeitsberechnungen; *Konstruktion* 20 (1968)7, pp. 245–251.
- [8] Siebel, E.; Stieler, M.: Ungleichförmige Spannungsverteilung bei schwingender Beanspruchung; *VDI-Zeitschrift* 97 (1955), pp. 121–126.
- [9] Kuguel, R.: A relation between theoretical stress concentration factor and fatigue notch factor deduced from the concept of high stressed volume; in *Proceedings 1961* (ASTM Ed.), 1961, pp. 732–744.
- [10] Leitner, M.: Local fatigue assessment of welded and high frequency mechanical impact treated joints, PhD thesis, Montanuniversität Leoben, 2013.
- [11] Stoschka, M.; Leitner, M.; Fössl, T.; Posch, G.: Effect of high-strength filler metals on fatigue; *Welding in the World* 56 (2012)3-4, pp. 20–29.
- [12] Stoschka, M.; Fössl, T.; Leitner, M.; Posch, G.: Contribution to the capability of filler metals to influence pulsating fatigue life, *IIW-Doc.: II-1742-10*, 2010.
- [13] Pitec GmbH: PIT (Pneumatic Impact Treatment). www.pitec-gmbh.com.
- [14] Leitner, M.; Stoschka, M.; Eichlseder, W.: Fatigue enhancement of thin-walled, high-strength steel joints by high-frequency mechanical impact treatment; *Welding in the World* 58 (2014)1, pp. 29–39.
- [15] ASTM E739: Practice for Statistical Analysis of Linear or Linearized Stress-Life (S-N) and Strain-Life (e-N) Fatigue Data, 2010.
- [16] Dengel, D.: Die arc sin \sqrt{P} -Transformation — ein einfaches Verfahren zur grafischen und rechnerischen Auswertung geplanter Wöhlersversuche; *Materialwissenschaft und Werkstofftechnik* 6 (1975)8, pp. 253–261.
- [17] Baumgartner, J.; Bruder, T.: An efficient meshing approach for the calculation of notch stresses; *Welding in the World* 57 (2013)1, pp. 137–145.
- [18] Sonsino, C. M.: Suggested allowable equivalent stresses for fatigue design of welded joints according to the notch stress concept with the reference radii $r_{ref} = 1.00$ and 0.05 mm, *IIW-Doc.: XIII-2216-08/XV-1285-08*, 2008.
- [19] Peterson, R. E.: Stress concentration design factors, Wiley, New York u.a., 1953.
- [20] Lawrence, F. V.; Ho, N. J.; Mazumdar, P. K.: Predicting the fatigue resistance of welds; *Annual Review of Materials Science* 11 (1981), pp. 401–425.
- [21] Radaj, D.: Design and analysis of fatigue resistant welded structures, Abington, Cambridge, England, 1990.
- [22] Radaj, D.: Ermüdungsfestigkeit, Springer, Berlin, 2003.
- [23] Forschungskuratorium Maschinenbau: Rechnerischer Festigkeitsnachweis für Maschinenbauteile aus Stahl, Eisenguss- und Aluminiumwerkstoffen, 2012.
- [24] Voestalpine GmbH: Alform®-Stähle: Technische Lieferbedingungen, 2011.
- [25] Zhang, G.; Sonsino, C. M.; Sundermeier, R.: Method of effective stress for fatigue: Part II – Applications to V-notches and seam welds; *International Journal of Fatigue* 37 (2012), pp. 24–40.